JCTC Journal of Chemical Theory and Computation

Updated Branching Plane for Finding Conical Intersections without Coupling Derivative Vectors

Satoshi Maeda,[†,‡,§] Koichi Ohno,*[,‡] and Keiji Morokuma*[,†,§]

Fukui Institute for Fundamental Chemistry, Kyoto University, Kyoto 606-8103, Japan, Toyota Physical and Chemical Research Institute, Nagakute, Aichi 480−1192, Japan, and Department of Chemistry and Cherry L. Emerson Center for Scientific Computation, Emory University, Atlanta, Georgia 30322

Received January 14, 2010

Abstract: The conical intersections (CIs) form a (*f*-2)-dimensional hyperspace on which two diabatic potential energy surfaces (PESs) belonging to the same symmetry cross, where *f* is the internal degree of freedom. The branching plane (BP) is a (two-dimensional) plane defined by the difference gradient vector (DGV) and the coupling derivative vector (CDV), and on the BP, the degeneracy of the two adiabatic PESs is lifted. The properties of the BP are often used in the exploration of the conical intersection hyperspace, such as determination of the minimum energy CI or the first-order saddle point in CI. Although both DGV and CDV are necessary to construct the BP in general, CDV is not always available depending on ab initio methods and programs. Therefore, we developed an approach for optimizing critical points on the CI hypersurface without CDV by using a BP updating method, which was shown to be accurate and very useful for minimum energy and saddle point optimization and for the minimum energy path following within the CI hypersurface in numerical tests for C_6H_6 and $C_5H_8N^+$.

1. Introduction

The conical intersections (CIs) form a (*f*-2)-dimensional hyperspace on which two diabatic potential energy surfaces (PESs) belonging to the same symmetry cross, where *f* is the internal degree of freedom. Conical intersections have been explored in a number of studies on photochemical and ion−molecule reactions, as regions where nonadiabatic transitions take place efficiently.[1−4] Especially, the minimum energy conical intersection (MECI) point is considered to be a critical point for nonadiabatic transition. Hence, there have been considerable efforts for developing efficient MECI optimization algorithms.[5−11] Furthermore, an automated systematic exploration method for MECIs has very recently been developed.[12] Recently, the first-order saddle point in CI hypersurface and the corresponding minimum energy path (MEP) were proposed to be important in dynamical trajectory simulations, and an optimization method was developed for such high-energy points within the CI hypersruface.[9]

The branching plane (BP) is a (two-dimensional) plane defined by the difference gradient vector (DGV) and the coupling derivative vector (CDV), and on the BP, the degeneracy of the two adiabatic PESs is lifted. The properties of BP are often used in the exploration of the CI hyperspace. Some of MECI optimizers use BP to keep degeneracy of two adiabatic states during optimizations.[6−9] The method for characterizing higher energy CI points also uses BP.[9] BP is required for finding transition directions in the generalized trajectory surface hopping method based on the Zhu−Nakamura theory,[13−15] in which the direction of CDV is estimated as the maximum eigenvalue direction of the difference Hessian matrix when CDV is not available.[13−15]

In order to use BP for optimization, both DGV and CDV vectors are necessary in every optimization step. DGV can be obtained easily from gradient vectors for two adiabatic PESs. If an analytical gradient is not available, it can be evaluated easily by numerical energy differentiation. However, CDV is

* Corresponding authors e-mail: ohnok@mail.tains.tohoku.ac.jp (K.O.); morokuma@emory.edu (K.M.).

† Kyoto University.

‡ Toyota Physical and Chemical Research Institute.

§ Department of Chemistry and Cherry L. Emerson Center for Scientific Computation.

10.1021/ct1000268
Published on Web 04/07/2010

not available for all ab initio methods, and programs since implementation of an analytical derivative method are required. When a new accurate ab initio method is developed, typically only the energy can be calculated, and the BP-based optimization method cannot be employed. In addition, it is sometimes better to avoid CDV calculations, if possible, because the cost for computing CDV is not negligible, especially for correlated ab initio methods.

To avoid CDV calculations, penalty function methods[10,11] have been developed and have been very useful for finding MECI regions using ab initio methods without CDV codes. However, convergence of these methods is, in general, slower than the BP-based method, especially if tight optimization for $(E_1 - E_2)$ is desired.[16] Therefore, often a very loose convergence criterion allowing large energy differences (usually larger than 1 kJ/mol) is employed for these methods. On the other hand, in the constrained optimization methods,[5,6,8] the constraint of the CDV direction can be omitted when CDV is not available, and this approach has also been employed together with correlated multireference methods without CDV codes,[17−19] although its convergence is slow when the mean energy gradient vector is highly coupling with the CDV direction.

Another possible approach for finding CIs without CDV is updating BP by using DGV, as has been done with the Hessian updating for single energy optimization. Many excellent Hessian updating methods have been developed for conventional augmented Hessian geometry optimizers.[20−24] BP is composed of only two vectors, and its updating should be much easier than updating Hessian of N atom systems with $3N - 6$ vectors. In the present paper, we propose a very simple method for updating BP. Although this BP-updating method can be combined with any BP-based optimization approach, we use it in combination with the gradient projection method, developed by Bearpark et al.[7] as an MECI optimizer and extended very recently by Sicilia et al.[9] for finding higher energy CI points. We demonstrate that the present update method gives very accurate BPs in CI regions and is very useful and efficient in locating minimum energy points, saddle points, and minimum energy paths in numerical tests for C_6H_6 and $C_5H_8N^+$.

2. Methods

2.1. Updating Branching Plane. The adiabatic energies for state 1 (E_1) and state 2 (E_2) can be written with the diabatic energies (U_{11} and U_{22}) and with their coupling U_{12}.

$$\begin{aligned} E_1 &= \frac{1}{2}(U_{11} + U_{22}) - \frac{1}{2}\sqrt{(U_{11} - U_{22})^2 + 4U_{12}^2} \\ E_2 &= \frac{1}{2}(U_{11} + U_{22}) + \frac{1}{2}\sqrt{(U_{11} - U_{22})^2 + 4U_{12}^2} \end{aligned} \tag{1}$$

Either when $U_{11} - U_{22} = U_{12} = 0$ is satisfied (on a CI) or when one assumed that the diabatic energies and their coupling is linearly dependent on any coordinate at the point of interest (in the first-order approximation of U_{nm}), the second derivative of $(E_1 - E_2)^2$ is given by

$$\frac{\partial^2 (E_1 - E_2)^2}{\partial x_i \partial x_j} = 2\left(\frac{\partial U_{11}}{\partial x_i} - \frac{\partial U_{22}}{\partial x_i}\right)\left(\frac{\partial U_{11}}{\partial x_j} - \frac{\partial U_{22}}{\partial x_j}\right) + 8\frac{\partial U_{12}}{\partial x_i}\frac{\partial U_{12}}{\partial x_j} \tag{2}$$

From eq 2, the second derivative matrix $\mathbf{H}$ of $(E_1 - E_2)^2$ can be written with two vectors $\mathbf{p}$ and $\mathbf{q}$ as

$$\mathbf{H} = 2\mathbf{p}\mathbf{p}^T + 8\mathbf{q}\mathbf{q}^T \tag{3}$$

where $\mathbf{p}$ is the DGV for diabatic energy with the component $\partial U_{11}/\partial x_i - \partial U_{22}/\partial x_i$ and $\mathbf{q}$ is the CDV for diabatic energy with the component $\partial U_{12}/\partial x_i$. Thus, $\mathbf{H}$ is given as a function of two vectors $\mathbf{p}$ and $\mathbf{q}$ and defines the BP. Here, adiabatic DGV and CDV can be written in terms of a linear combination of $\mathbf{p}$ and $\mathbf{q}$, since BP does not change by a diabatic to adiabatic transformation. Although diabatic DGV and CDV and adiabatic DGV and CDV are used together in the following explanation, BP can be defined by any combination of these four vectors because they all are vectors on a common BP.

We express BP at the kth optimization step by two vectors $\mathbf{x}_k$ and $\mathbf{y}_k$, where these are an unit vector parallel to DGV for adiabatic energy at the kth step and an unit vector on BP perpendicular to $\mathbf{x}_k$, respectively. Here, at the kth step, $\mathbf{x}_{k-1}$, $\mathbf{y}_{k-1}$, and $\mathbf{x}_k$ are known, and $\mathbf{y}_k$ is an unknown vector to be estimated by the BP updating method. In the first-order approximation ($\partial^2 U_{nm}/\partial x_i \partial x_j = 0$), it is obvious that BP (i.e., $\mathbf{p}$ and $\mathbf{q}$ in eq 3) does not change by any geometry displacement because $\partial U_{nm}/\partial x_i$, which are elements of $\mathbf{p}$ and $\mathbf{q}$ shown in eq 2, is independent of x_i. Thus the first-order BP at the kth step is nothing but a plane defined by $\mathbf{x}_{k-1}$ and $\mathbf{y}_{k-1}$. Let us consider $\mathbf{x}_k$ has been obtained exactly without the first-order approximation. Thus $\mathbf{x}_k$ may have a component not contained in $\mathbf{x}_{k-1}$ or $\mathbf{y}_{k-1}$ because of the higher order terms in determining $\mathbf{x}_k$. The value of $\mathbf{y}_k$ can be estimated by the unchanged first-order BP: such a $\mathbf{y}_k$ should be written by a linear combination of $\mathbf{x}_{k-1}$ and $\mathbf{y}_{k-1}$ as $\mathbf{y}_k = \alpha\mathbf{x}_{k-1} + \beta\mathbf{y}_{k-1}$. Since $\mathbf{y}_k$ is a unit vector orthogonal to $\mathbf{x}_k$, we get the following simultaneous equations for α and β:

$$\begin{aligned} \alpha(\mathbf{x}_{k-1}\cdot\mathbf{x}_k) + \beta(\mathbf{y}_{k-1}\cdot\mathbf{x}_k) &= 0 \\ \alpha^2 + \beta^2 &= 1 \end{aligned} \tag{4}$$

Then, by solving eq 4, we obtain $\mathbf{y}_k$ as

$$\mathbf{y}_k = \frac{(\mathbf{y}_{k-1}\cdot\mathbf{x}_k)\mathbf{x}_{k-1} - (\mathbf{x}_{k-1}\cdot\mathbf{x}_k)\mathbf{y}_{k-1}}{\sqrt{(\mathbf{y}_{k-1}\cdot\mathbf{x}_k)^2 + (\mathbf{x}_{k-1}\cdot\mathbf{x}_k)^2}} \tag{5}$$

This $\mathbf{y}_k$ is used together with $\mathbf{x}_k$ for constructing the updated BP at the kth step, and they are stored either in memory or in disk for the next step. At the initial step, one does not have the first-order BP ($\mathbf{x}$ and $\mathbf{y}$ at the last step). A plane for $\mathbf{x}_0$ and the mean energy gradient vector was used as an initial BP in this study. Such a BP is exact at stationary points in CIs, since the mean energy gradient vector does not contain any components perpendicular to BP at such points. Thus CDV is no longer necessary at every optimization step when this BP updating algorithm is employed. Although this scheme partly assumes the first-order ap-

proximation of U_{nm}, higher-order effects are accounted for by using the exact $\mathbf{x}_k$, and it worked very well in numerical tests shown below.

As shown in the following test calculations, *updated* $\mathbf{y}_k$ using eq 5 converges to a very accurate one around CI regions, even if an initial $\mathbf{y}_0$ is very poor. This can be understood by considering an optimization step around an apex of cone. When *updated* $\mathbf{y}_{k-1}$ is not very accurate and the mean energy gradient vector has a component of *true* $\mathbf{y}_{k-1}$, an optimization step there will have a component of *true* $\mathbf{y}_{k-1}$, in addition to a component of $\mathbf{x}_{k-1}$. The component of $\mathbf{x}_{k-1}$ minimizes the energy difference, whereas the component of *true* $\mathbf{y}_{k-1}$ increases the energy difference. In other words, the component of $\mathbf{x}_{k-1}$ heads toward the apex, whereas the component of *true* $\mathbf{y}_{k-1}$ leaves the apex behind. Consequently, $\mathbf{x}_k$ becomes very similar to *true* $\mathbf{y}_{k-1}$, and *true* $\mathbf{y}_k$ becomes very similar to $\mathbf{x}_{k-1}$. Here, except for the case where *updated* $\mathbf{y}_{k-1}$ is orthogonal to *true* $\mathbf{y}_{k-1}$, *updated* $\mathbf{y}_k$ by eq 5 becomes very similar to $\mathbf{x}_{k-1}$ and *true* $\mathbf{y}_k$. In the final stage, optimizations keep walking around the apex of cone, and $\mathbf{y}_k$ can be purified to a very accurate one by eq 5 because of accompanying rotations of $\mathbf{x}$ around the apex of cone. Here, based on this discussion, one can assume a simpler algorithm using a plane of $\mathbf{x}_{k-1}$ and $\mathbf{x}_k$ as an updated BP. However, this algorithm was numerically unstable in our tests when $\mathbf{x}_k$ is very similar to $\mathbf{x}_{k-1}$, and it can be stabilized by adding $\mathbf{y}_{k-1}$ to the plane of $\mathbf{x}_{k-1}$ and $\mathbf{x}_k$ with a certain amount as eq 5.

As can be seen in the above discussion, the present BP updating is a technique to obtain an accurate BP using rotations of $\mathbf{x}$ induced by a walk at a finite distance from CI. Hence, this does not work for special systems, such as symmetry required Jahn−Teller systems, because one can walk exactly on CI using symmetry. However, in such systems, BP is not required in optimizations because there is no need to keep geometry on CI by using BP. Moreover, the present BP updating should work in Jahn−Teller systems too when optimizations start from a lower symmetry point and when no symmetry related constraint is employed. On the other hand, no rotation of $\mathbf{x}$ occurs when a seam between two states with different symmetry or when spin-multiplicity as the norm of CDV is zero. Although the BP updating does not work in this case too, BP is not necessary because $\mathbf{x}$ is only direction to increase the energy difference. It follows that the present BP updating is expected to work many systems in which BP is required in optimizations.

2.2. The Gradient Projection Method. In the gradient projection method, the following gradient vector is employed in optimizations:[7,9]

$$\mathbf{g} = \mathbf{g}'_{\mathrm{diff}} + \mathbf{P}\mathbf{g}_{\mathrm{mean}} \tag{6}$$

where $\mathbf{g}'_{\mathrm{diff}} = 2(E_1 - E_2)\mathbf{x}$, $\mathbf{g}_{\mathrm{mean}}$ is the mean energy gradient vector, and $\mathbf{P}$ is the following projection matrix:

$$\mathbf{P} = \mathbf{1} - \mathbf{x}\mathbf{x}^T - \mathbf{y}\mathbf{y}^T \tag{7}$$

Here, a unit vector parallel to CDV is used instead of $\mathbf{y}$ in the original expression of $\mathbf{P}$,[7,9] which is identical to $\mathbf{P}$ of eq 7. On the CI hypersurface, the condition $|\mathbf{g}'_{\mathrm{diff}}| = 0$ is fulfilled at all points, and points with $|\mathbf{g}'_{\mathrm{diff}}| = |\mathbf{P}\mathbf{g}_{\mathrm{mean}}| = 0$ correspond to stationary points. A geometry displacement toward the inverse direction of the gradient vector minimizes the $(E_1 + E_2)/2$ function in the $3N - 8$ dimensional intersection space and minimizes the $(E_1 - E_2)^2/\alpha$ function in the two-dimensional branching space, where α is the norm of DGV. The use of $(E_1 - E_2)^2/\alpha$, rather than $(E_1 - E_2)^2$ itself, is better because $1/\alpha$ serves as a parameter that scales energy units and weight and improves the performance.

Treatment of Hessian is very tricky when the gradient of eq 6 is combined to augmented Hessian methods, such as the Newton−Raphson method.[9] Here, we describe only a procedure we used in this study, which is similar to a treatment of Sicilia et al.[9] in CI regions. Among normal modes for augmented Hessian methods, $3N - 8$ are nonzero eigenvalue modes of the projected mean energy Hessian $\mathbf{P}\mathbf{H}_{\mathrm{mean}}\mathbf{P}$. Another is $\mathbf{x}$ with corresponding eigenvalue 2α. Only these $3N - 7$ modes are used because optimization steps are always perpendicular to the remaining $\mathbf{y}$, as the gradient of eq 6 does not contain components of $\mathbf{y}$. This set of modes and eigenvalues gives exact second-order steps in CIs, as long as $\mathbf{H}_{\mathrm{mean}}$ is exact.

It is easy to combine the gradient projection method with the minimum energy path (MEP) following methods for single PES.[25−28] We employed the second-order algorithm which was proposed by Page and McIver[26] and is employed in Gaussian09[29] for predictor steps.[28] Although combining the corrector step in Gaussian09 to the gradient projection method will improve performance of the MEP following, it is beyond the scope of this study. We simply used the above-mentioned set of normal modes and eigenvalues as normal modes for the second-order algorithm. Since such second-order steps sometime caused unacceptably large energy differences of >5 kJ/mol, $(E_1 - E_2)^2$ was minimized along DGV until $|E_1 - E_2| < 0.1$ kJ/mol was met.

2.3. Computation. In the present study, the rational function optimization (RFO) method[30] was employed in combination with the gradient projection method[7,9] for obtaining each optimization step. Such optimizations were performed in the Cartesian coordinates throughout. $\mathbf{H}_{\mathrm{mean}}$ was updated by using $\mathbf{g}_{\mathrm{mean}}$ at the current and last optimization steps, where combined BFGS[20] and SR1[21] methods[24] were used in the minimization and combined Powell[22] and SR1 methods[23] were employed in the saddle point optimization and the MEP following. All the test calculations have been performed at the SA-CASSCF level of theory, where a two π electron and two π orbital active space and an STO-3G basis set were employed unless mentioned. Energy, gradient, and CDV were computed by using the Gaussian09 programs.[29] Optimizations were considered to be converged when the following four conditions are met simultaneously: (i) the maximum gradient is smaller than 3.0×10^{-4} hartree Å^{-1}; (ii) the root-mean-square (rms) gradient is smaller than 2.0×10^{-4} hartree Å^{-1}; (iii) the maximum displacement is smaller than 1.5×10^{-3} Å; and (iv) the rms displacement is smaller than 1.0×10^{-3} Å. These algorithms were implemented in the GRRM program developed by the authors for

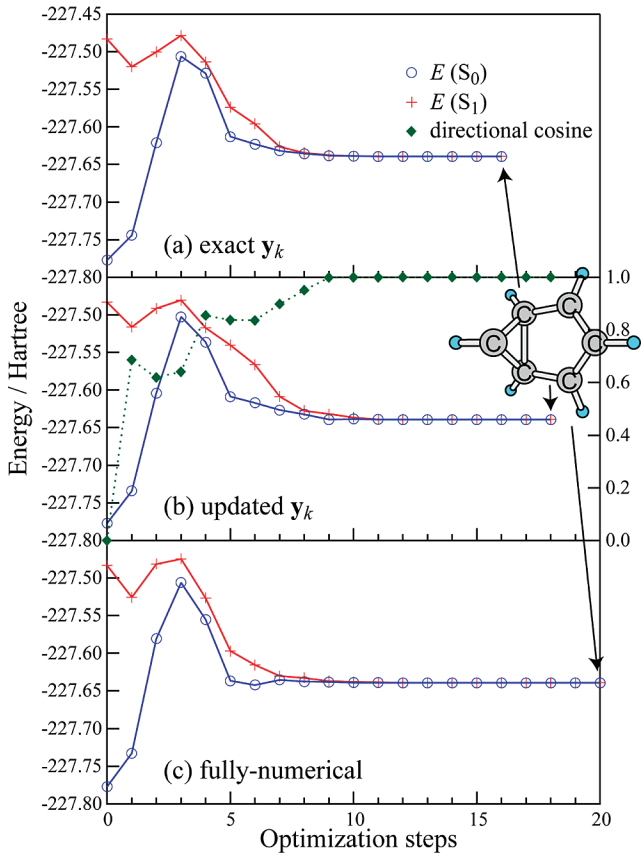

Figure 1. Energy profiles along three different optimizations for MECI of C_6H_6 (benzene): (a) using analytical DGV and exact $\mathbf{y}_k$, (b) using analytical DGV and updated $\mathbf{y}_k$, and (c) using numerical DGV and updated $\mathbf{y}_k$ (fully numerical). Energies for S_1 and S_0 states are plotted by + and ○, respectively. Plots (♦) of directional cosine values between exact and updated $\mathbf{y}_k$ during the optimization with updated $\mathbf{y}_k$ are superimposed on (b). Energy gaps at the final points in optimizations (a−c) are 0.0000, 0.0003, and 0.1187 kJ/mol, respectively.

automated global reaction route mapping on PESs,[31−33] and all geometry displacements were treated by the GRRM program.

3. Numerical Tests

3.1. Optimization of MECI. Tests are made for three known S_0/S_1 MECIs for C_6H_6 (benzene[34] and fulbene)[35] and $C_5NH_8^+$ (a model species of protonated retinal,[36] CH_2═CH−CH═CH−CH═NH^+).

Figure 1 shows energy profiles along three different optimizations for MECI of C_6H_6 (benzene): (a) using analytical DGV and exact $\mathbf{y}_k$; (b) using analytical DGV and updated $\mathbf{y}_k$; and (c) using numerical DGV and updated $\mathbf{y}_k$ (fully numerical), where numerical DGVs were evaluated by forward and backward single-point energy samplings in the Cartesian coordinates with a step size of 0.005 Å. The initial structure was prepared by a RHF/STO-3G constrained optimization, fixing one CCCC dihedral angle of benzene at 75°. The initial $\mathbf{H}_{\text{mean}}$ is the ground-state Hessian of the RHF/STO-3G method at the initial structure. Although (a) converged most quickly among the three, (b) and (c) are not very slow compared to (a) with only a few extra optimization steps. To see the accuracy of the updated BP in each optimization step, we plotted values of directional cosine between exact and updated $\mathbf{y}_k$ in Figure 1b, along the optimization profile of (b), where the value is unity if an updated $\mathbf{y}_k$ is exact, whereas it is zero if perpendicular to an exact $\mathbf{y}_k$. Although updated $\mathbf{y}_k$ was not very accurate at the initial stage because of a poor initial BP, it was improved substantially with optimization steps. Degeneracy of the two states was almost reached around the 10th step, and updated $\mathbf{y}_k$ was especially accurate from the 10th step with the values larger than 0.99. This is because eq 5 was formulated from eq 2 which is a second-order formula only at CIs. Inaccurate $\mathbf{y}_k$ in the initial stage of (b) remained only in two more optimization steps compared to (a). This is because $\mathbf{y}_k$ is not very important far from CIs, since adiabatic PESs have the cone-shaped square-root topology only around CI regions. The fully numerical optimization (c) is also performed to demonstrate that the present method allows BP-based optimizations using single-point energy only calculations, although this calculation gave a larger energy gap than those in (a) and (b) because of numerical errors in the numerical differentiations of single-point energies.

Fulbene, an isomer of benzene, is a good benchmark of CI optimizers since there are many low-lying critical points in its CI.[35] Although many early works[37,38] failed to locate true MECI and reported first- and second-order saddle-points to be MECI. The true MECI was discovered by very careful analyses in the CI hyperspace using the intersection-space Hessian approach.[35] Hence, in this test, we prepared different initial structures in the potential basin of fulbene to see the radius of convergence of the present optimizer. Here, we employed a six π electron and six π orbital active-space and the Dunning cc-pVDZ basis set so that obtained structures can be compared to the MECI reported in ref 35. In both optimizations, the present BP updating method was employed. Figure 2 shows energy profiles along two optimizations starting from two different structures. In the optimization (a), the initial structure was prepared by a RHF/STO-3G constrained optimization fixing a CC═CH dihedral angle at 75°, where CC of the CC═CH are atoms in the five-membered ring and the remaining CH are atoms in the ═CH_2 group of fulbene. In the optimization (b), the initial structure was prepared by a RHF/STO-3G constrained optimization fixing the CC═CH dihedral angle at 5°. The initial $\mathbf{H}_{\text{mean}}$ are ground-state Hessian of the RHF/STO-3G method at these initial structures. As seen in Figure 2, both optimizations converged to the same MECI with C_1 symmetry reported in ref 35, where average electronic energies of the final structures in optimizations (a) and (b) are −230.6513948 and −230.6513947 hartree, respectively, which are very similar to the reported value (−230.6513957) in ref 35. Although there is an energy bump in the profile (b), due to a significant change in molecular orbitals of CASSCF at the point, the optimization finally converged to the correct MECI. Among the two initial structures, one with the CC═CH dihedral angle equal to 75° is closer to the MECI than that of the other. Consequently, the optimization (a) converged much more quickly than (b). Although there is a planar second-order saddle-point with C_{2v} symmetry

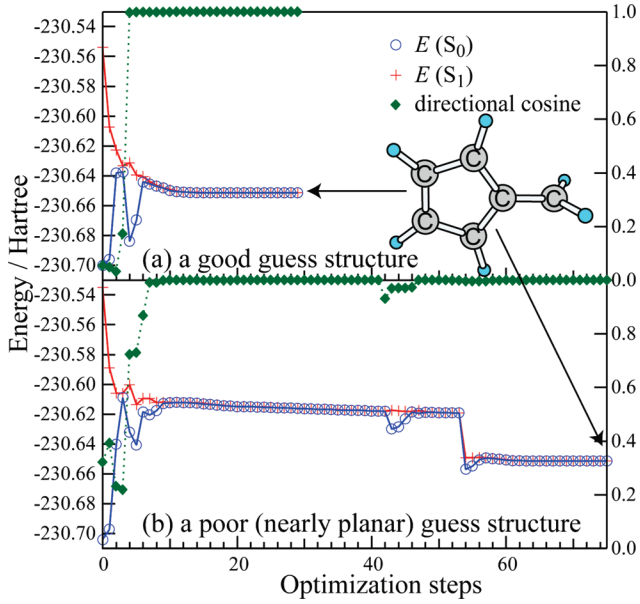

Figure 2. Energy profiles along two different optimizations for MECI of C_6H_6 (fulbene) using analytical DGV and updated $\mathbf{y}_k$: (a) starting from a good initial structure and (b) starting from a poor (nearly planar) initial structure. Energies for S_1 and S_0 states are plotted by + and ○, respectively. Plots (♦) of directional cosine values between exact and updated $\mathbf{y}_k$ are superimposed. Energy gaps at the final points in optimizations (a) and (b) are 0.0016 and 0.0026 kJ/mol, respectively.

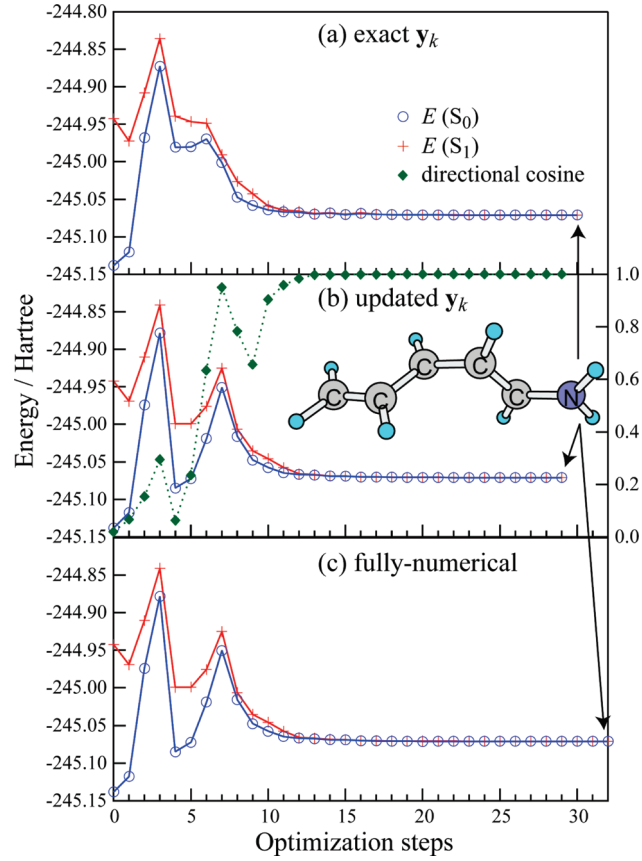

Figure 3. Energy profiles along three different optimizations for MECI of $C_5H_8N^+$: (a) using analytical DGV and exact $\mathbf{y}_k$, (b) using analytical DGV and updated $\mathbf{y}_k$, and (c) using numerical DGV and updated $\mathbf{y}_k$ (fully numerical). Energies for S_1 and S_0 states are plotted by + and ○, respectively. Plots (♦) of directional cosine values between exact and updated $\mathbf{y}_k$ during the optimization with updated $\mathbf{y}_k$ are superimposed on (b). Energy gaps at the final points in optimizations (a−c) are 0.0005, 0.0045, and 0.0819 kJ/mol, respectively.

close to the second initial structure,[35] the optimization (b) converged to the true MECI structure because of the proper step contorting by the RFO method. As seen in the figure, values of directional cosine between exact and updated $\mathbf{y}_k$ are very close to unity in CI regions.

Figure 3 shows results for $C_5NH_8^+$. Optimizations (a−c) are similar to those for benzene (Figure 1). The initial structure was prepared by RHF/STO-3G constrained optimizations fixing the central CCCC dihedral angle of $CH_2{=}CH{-}CH{=}CH{-}CH{=}NH^+$ at 75°. The initial $\mathbf{H}_{\text{mean}}$ is ground-state Hessian of the RHF/STO-3G method at the initial structure. The numbers of optimization steps are similar among the three different optimizations. Although updated $\mathbf{y}_k$ was not accurate in the initial stage, it was very accurate after degeneracy was reached around the 15th step. The errors in the initial stage did not strongly affect the total number of optimization steps.

3.2. Determination of Saddle-Point and MEP within the CI Hypersurface. We performed a saddle-point optimization and a corresponding MEP calculation within the CI hypersurface for C_6H_6 to show that the BP updating method works also for higher energy CI points. The initial structure for the saddle-point optimization was prepared by a RHF/STO-3G constrained optimization fixing a CC bond length at 1.853 Å and a CCCC dihedral angle at 90°, where the CC bond is a newly generated bond for the three-membered ring in the MECI of Figure 1, and the CCCC dihedral angle is the one fixed in the initial structure preparation for the MECI optimization. Although this structure was prepared intending to find a saddle-point located in a reaction coordinate related to a deformation of C_6 backbone (mainly related to the CC dimer rotation), there is no such saddle-point, and another saddle-point was discovered as shown below. The initial $\mathbf{H}_{\text{mean}}$ is the ground-state Hessian of the RHF/STO-3G method at the initial structure.

Figure 4 shows energy profiles along two different optimizations for a saddle point in CI of C_6H_6: (a) using analytical DGV and exact $\mathbf{y}_k$, and (b) using analytical DGV and updated $\mathbf{y}_k$. In this case, (b) accidentally converged slightly faster than (a). Although the initial $\mathbf{H}_{\text{mean}}$ did not have any negative eigenvalue modes, these optimizations finally converged to a saddle point by walking along the lowest frequency mode. Hence, most parts of the profiles are uphill, and consequently, these optimizations needed as much as 130 steps. The gradient projection method found the CI region very quickly within 10 optimization steps, after which the updated $\mathbf{y}_k$ was very accurate. It should be noted that this example is demonstrating robustness of the RFO method in first-order saddle-point optimizations in the CI hypersurface, starting from a poor initial guess and an inaccurate $\mathbf{H}_{\text{mean}}$. As has been shown in optimizations of single PESs, augmented Hessian methods, such as the RFO

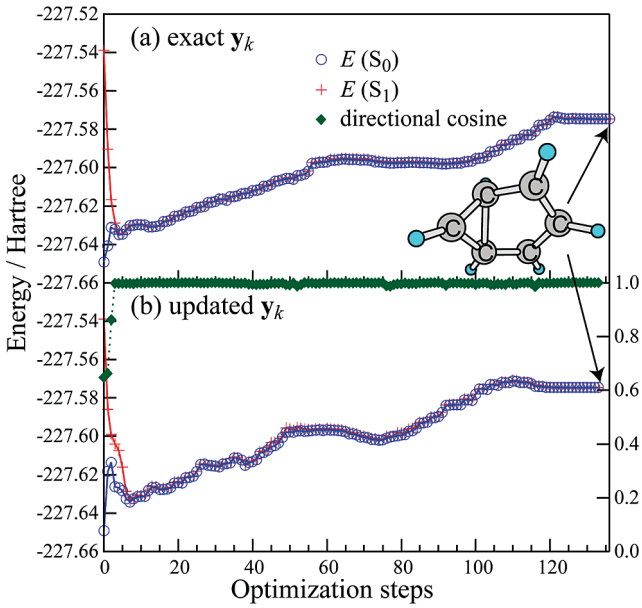

Figure 4. Energy profiles along two different optimizations for a saddle point in CI of C_6H_6: (a) using analytical DGV and exact $\mathbf{y}_k$ and (b) using analytical DGV and updated $\mathbf{y}_k$. Energies for S_1 and S_0 states are plotted by + and ○, respectively. Plots (♦) of directional cosine values between exact and updated $\mathbf{y}_k$ during the optimization with updated $\mathbf{y}_k$ are superimposed on (b). Energy gaps at the final points in optimizations (a) and (b) are 0.0021 and 0.0037 kJ/mol, respectively.

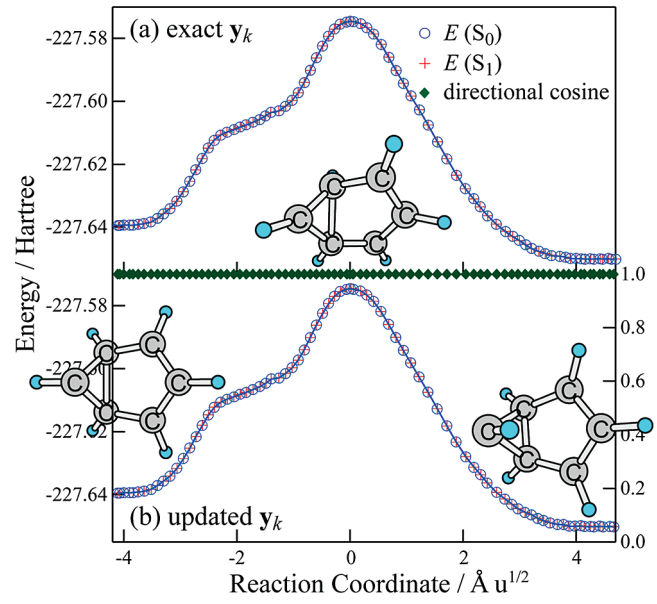

Figure 5. Energy profiles along a MEP in CI of C_6H_6 traced by two different algorithms: (a) using analytical DGV and exact $\mathbf{y}_k$ and (b) using analytical DGV and updated $\mathbf{y}_k$. Energies for S_1 and S_0 states are plotted by + and ○, respectively. Plots (♦) of directional cosine values between exact and updated $\mathbf{y}_k$ during the MEP calculation with updated $\mathbf{y}_k$ are superimposed on (b). Energy gaps at the end points of the MEPs are (a-left) 0.0018, (a-right) 0.0005, (b-left) 0.0029, and (b-right) 0.0011 kJ/mol.

method, greatly expand the radius of convergence of transition-state optimizations.[39]

Starting from the first-order saddle point within the CI hypersurface obtained by this optimization, a MEP was calculated in the mass weighted Cartesian coordinate, where a step size (in Å $u^{1/2}$) was adjusted so that a simple linear displacement along the inverse gradient vector is equal to 0.1 Å in each step. In the MEP following, $\mathbf{H}_{mean}$ was computed once at the initial structure by numerical differentiations of $\mathbf{g}_{mean}$ to define the negative eigenvalue mode to be followed. Here, the projected $\mathbf{H}_{mean}$ ($\mathbf{PH}_{mean}\mathbf{P}$) has only one negative eigenvalue mode, which is confirming that the point is a first-order saddle point in the CI hypersurface. Here, this procedure using $\mathbf{PH}_{mean}\mathbf{P}$ is based on the first-order approximation of CI hyperspace, which may cause a large energy gap in the initial MEP integration step. Use of the intersection-space Hessian defined by Sicilia et al.[35,40] gives a more accurate initial reaction coordinate direction. Nevertheless, the present procedure gave a reasonable MEP passing through a space with a very small energy gap, as shown below because of the minimization of $(E_1 - E_2)^2$ in every integration point.

Figure 5 shows energy profiles along an MEP in the CI hypersurface of C_6H_6 by two different calculations, starting from the saddle point of Figure 4: (a) using analytical DGV and exact $\mathbf{y}_k$, and (b) using analytical DGV and updated $\mathbf{y}_k$. These two MEP calculations gave exactly the same connection which is between the MECI in Figure 1 and a lower energy MECI with a different CH direction. Energy differences between two states are always smaller than 0.1 kJ/mol along these profiles (overlapping in the figure) because of the minimizations of $(E_1 - E_2)^2$. The updated $\mathbf{y}_k$ was very accurate, and the directional cosine between exact and updated $\mathbf{y}_k$ was larger than 0.9999 at all points. Here, $\mathbf{y}_0$ at the initial step (at 0 Å $u^{1/2}$) was already very accurate with the directional cosine of 0.99994 because the initial BP for $\mathbf{x}_0$, and the mean gradient vector is exact at stationary points in the CI hypersurface.

4. Conclusion

We proposed a very simple method for updating branching plane (BP) by using a difference gradient vector (DGV) at the current position and (either exact or approximate) BP at the last position. In this study, we combined it with the gradient projection method to look into its performance not only around minimum energy conical intersections (MECIs) but also in higher energy CI points, although it is straightforward to combine it with other BP-based MECI optimizers in principle. In spite of a very simple assumption in the BP updating formula, updated BPs were very accurate in both low- and high-energy CI regions, as shown in numerical tests for C_6H_6 and $C_5H_8N^+$. Thus, the present method can be a powerful tool for finding CIs when the coupling derivative vector (CDV) is not available. Since the use of updated BPs did not increase the total numbers of optimization steps in the numerical tests, it can reduce computation demands for CDV calculations as well.

Acknowledgment. S.M. is supported by a Research Fellowship from the Japan Society for Promotion of Science for Young Scientists. This work is partly supported by a grant from the Japan Science and Technology Agency with a Core

Research for Evolutional Science and Technology (CREST) in the area of high performance computing for multiscale and multiphysics phenomena as well as a grant from AFOSR (Grant no. FA9550-07−1-0395). The computational resources at the Research Center for Computational Science at Institute for Molecular Science are gratefully acknowledged.

References

(1) Bernardi, F.; Olivucci, M.; Robb, M. A. Potential Energy Surface Crossings in Organic Photochemistry. *Chem. Soc. Rev.* **1996**, *25*, 321.

(2) Yarkony, D. R. Conical Intersections: Diabolical and Often Misunderstood. *Acc. Chem. Res.* **1998**, *31*, 511.

(3) Sobolewski, A. L.; Domcke, W.; Dedonder-Lardeux, C.; Jouvet, C. Excited-State Hydrogen Detachment and Hydrogen Transfer Driven by Repulsive $1\pi\sigma^*$ States: A New Paradigm for Nonradiative Decay in Aromatic Biomolecules. *Phys. Chem. Chem. Phys.* **2002**, *4*, 1093.

(4) Levine, B. G.; Martínez, T. J. Isomerization through Conical Intersections. *Annu. Rev. Phys. Chem.* **2007**, *58*, 613.

(5) Koga, N.; Morokuma, K. Determination of the Lowest Energy Point on the Crossing Seam between Two Potential Surfaces Using the Energy Gradient. *Chem. Phys. Lett.* **1985**, *119*, 371.

(6) Manaa, M. R.; Yarkony, D. R. On the Intersection of Two Potential Energy Surfaces of the Same Symmetry. Systematic Characterization Using a Lagrange Multiplier Constrained Procedure. *J. Chem. Phys.* **1993**, *99*, 5251.

(7) Bearpark, M. J.; Robb, M. A.; Schlegel, H. B. A Direct Method for the Location of the Lowest Energy Point on a Potential Surface Crossing. *Chem. Phys. Lett.* **1994**, *223*, 269.

(8) Anglada, J. M.; Bofill, J. M. A Reduced-Restricted-Quasi-Newton-Raphson Method for Locating and Optimizing Energy Crossing Points between Two Potential Energy Surfaces. *J. Comput. Chem.* **1997**, *18*, 992.

(9) Sicilia, F.; Blancafort, L.; Bearpark, M. J.; Robb, M. A. New Algorithms for Optimizing and Linking Conical Intersection Points. *J. Chem. Theor. Comput.* **2008**, *4*, 257.

(10) Ciminelli, C.; Granucci, G.; Persico, M. The Photoisomerization Mechanism of Azobenzene: A Semiclassical Simulation of Nonadiabatic Dynamics. *Chem.—Eur. J.* **2004**, *10*, 2327.

(11) Levine, B. G.; Coe, J. D.; Martínez, T. J. Optimizing Conical Intersections without Derivative Coupling Vectors: Application to Multistate Multireference Second-Order Perturbation Theory (MS-CASPT2). *J. Phys. Chem. B* **2008**, *112*, 405.

(12) Maeda, S.; Ohno, K.; Morokuma, K. Automated Global Mapping of Minimal Energy Points on Seams of Crossing by the Anharmonic Downward Distortion Following Method: A Case Study of H_2CO. *J. Phys. Chem. A* **2009**, *113*, 1704.

(13) Oloyede, P.; Mil'nikov, G.; Nakamura, H. Generalized Trajectory Surface Hopping Method Based on the Zhu-Nakamura Theory. *J. Chem. Phys.* **2006**, *124*, 144110.

(14) Nakamura, H. Dynamics of Nonadiabatic Chemical Reactions. *J. Phys. Chem. A* **2006**, *110*, 10929.

(15) Nakamura, H. Nonadiabatic Chemical Dynamics: Comprehension and Control of Dynamics, and Manifestation of Molecular Functions. *Adv. Chem. Phys.* **2008**, *138*, 95.

(16) Keal, T. W.; Koslowski, A.; Thiel, W. Comparison of Algorithms for Conical Intersection Optimisation Using Semiempirical Methods. *Theor. Chem. Acc.* **2007**, *118*, 837.

(17) Zhang, P.; Irle, S.; Morokuma, K.; Tschumper, G. S. Ab Initio Theoretical Studies of Potential Energy Surfaces in the Photodissociation of the Vinyl Radical. I. Ã State Dissociation. *J. Chem. Phys.* **2003**, *119*, 6524.

(18) Serrano-Andrés, L.; Merchán, M.; Lindh, R. Computation of Conical Intersections by Using Perturbation Techniques. *J. Chem. Phys.* **2005**, *122*, 104107.

(19) Zhang, P.; Maeda, S.; Morokuma, K.; Braams, B. J. Photochemical Reactions of the Low-Lying Excited States of Formaldehyde: T_1/S_0 Intersystem Crossings, Characteristics of the S_1 and T_1 Potential Energy Surfaces, and a Global T_1 Potential Energy Surface. *J. Chem. Phys.* **2009**, *130*, 114304.

(20) (a) Broyden, C. G. The Convergence of a Class of Double-rank Minimization Algorithms 1. General Considerations. *J. Inst. Math. Its Appl.* **1970**, *6*, 76. (b) Fletcher, R. A New Approach to Variable Metric Algorithms. *Comput. J. (Switzerland)* **1970**, *13*, 317. (c) Goldfarb, D. A Family of Variable-Metric Methods Derived by Variational Means. *Math. Comput.* **1970**, *24*, 23. (d) Shanno, D. F. Conditioning of Quasi-Newton Methods for Function. *Math. Comput.* **1970**, *24*, 647.

(21) Murtagh, B.; Sargent, R. W. H. Computational Experience with Quadratically Convergent Minimisation Methods. *Comput. J. (Switzerland)* **1972**, *13*, 185.

(22) Powell, M. J. D. Recent Advances in Unconstrained Optimization. *Math. Program.* **1971**, *1*, 26.

(23) Bofill, J. M. Updated Hessian Matrix and the Restricted Step Method for Locating Transition Structures. *J. Comput. Chem.* **1994**, *15*, 1.

(24) Farkas, Ö.; Schlegel, H. B. Methods for Optimizing Large Molecules. II. Quadratic Search. *J. Chem. Phys.* **1999**, *111*, 10806.

(25) Ishida, K.; Morokuma, K.; Komornicki, A. The Intrinsic Reaction Coordinate. An Ab Initio Calculation for HNC→HCN and $H^- + CH_4 \rightarrow CH_4 + H^-$. *J. Chem. Phys.* **1977**, *66*, 2153.

(26) Page, M.; McIver, J. W., Jr. On Evaluating the Reaction Path Hamiltonian. *J. Chem. Phys.* **1988**, *88*, 922.

(27) Gonzalez, C.; Schlegel, H. B. An Improved Algorithm for Reaction Path Following. *J. Chem. Phys.* **1989**, *90*, 2154.

(28) Hratchian, H. P.; Schlegel, H. B. Using Hessian Updating to Increase the Efficiency of a Hessian based Predictor-Corrector Reaction Path Following Method. *J. Chem. Theory Comput.* **2005**, *1*, 61.

(29) Frisch, M. J.; Trucks, G. W.; Schlegel, H. B.; Scuseria, G. E.; Robb, M. A.; Cheeseman, J. R.; Scalmani, G.; Barone, V.; Mennucci, B.; Petersson, G. A.; Nakatsuji, H.; Caricato, M.; Li, X.; Hratchian, H. P.; Izmaylov, A. F.; Bloino, J.; Zheng, G.; Sonnenberg, J. L.; Hada, M.; Ehara, M.; Toyota, K.; Fukuda, R.; Hasegawa, J.; Ishida, M.; Nakajima, T.; Honda, Y.; Kitao, O.; Nakai, H.; Vreven, T.; Montgomery, J. A., Jr.; Peralta, J. E.; Ogliaro, F.; Bearpark, M.; Heyd, J. J.; Brothers, E.; Kudin, K. N.; Staroverov, V. N.; Kobayashi, R.; Normand, J.; Raghavachari, K.; Rendell, A.; Burant, J. C.; Iyengar, S. S.; Tomasi, J.; Cossi, M.; Rega, N.; Millam, J. M.; Klene, M.; Knox, J. E.; Cross, J. B.; Bakken, V.; Adamo, C.; Jaramillo, J.; Gomperts, R.; Stratmann, R. E.; Yazyev, O.; Austin, A. J.; Cammi, R.; Pomelli, C.; Ochterski, J. W.; Martin, R. L.; Morokuma, K.; Zakrzewski, V. G.; Voth, G. A.; Salvador, P.; Dannenberg, J. J.; Dapprich, S.; Daniels, A. D.; Farkas, O.; Foresman, J. B.; Ortiz, J. V.; Cioslowski, J.; Fox, D. J. *Gaussian 09*, revision A.1; Gaussian, Inc.: Wallingford, CT, 2009.

(30) Banerjee, A.; Adams, N.; Simons, J.; Shepard, R. Search for Stationary Points on Surfaces. *J. Phys. Chem.* **1985**, *89*, 52.

(31) Ohno, K.; Maeda, S. A Scaled Hypersphere Search Method for the Topography of Reaction Pathways on the Potential Energy Surface. *Chem. Phys. Lett.* **2004**, *384*, 277.

(32) Maeda, S.; Ohno, K. Global Mapping of Equilibrium and Transition Structures on Potential Energy Surfaces by the Scaled Hypersphere Search Method: Applications to ab Initio Surfaces of Formaldehyde and Propyne Molecules. *J. Phys. Chem. A* **2005**, *109*, 5742.

(33) Ohno, K.; Maeda, S. Global Reaction Route Mapping on Potential Energy Surfaces of Formaldehyde, Formic Acid, and Their Metal-Substituted Analogues. *J. Phys. Chem. A* **2006**, *110*, 8933.

(34) Palmer, I. J.; Ragazos, I. N.; Bernardi, F.; Olivucci, M.; Robb, M. A. An MC-SCF Study of the S_1 and S_2 Photochemical-Reactions of Benzene. *J. Am. Chem. Soc.* **1993**, *115*, 673.

(35) Sicilia, F.; Bearpark, M. J.; Blancafort, L.; Robb, M. A. An Analytical Second-Order Description of the S_0/S_1 Intersection Seam: Fulvene Revisited. *Theor. Chem. Acc.* **2007**, *118*, 241.

(36) Garavelli, M.; Celani, P.; Bernardi, F.; Robb, M. A.; Olivucci, M. The $C_5H_6NH_2^+$ Protonated Shiff Base: An Ab Initio Minimal Model for Retinal Photoisomerization. *J. Am. Chem. Soc.* **1997**, *119*, 6891.

(37) Dreyer, J.; Klessinger, M. Excited States and Photochemical Reactivity of Fulvene. A Theoretical Study. *J. Chem. Phys.* **1994**, *101*, 10655.

(38) Deeb, O.; Cogan, S.; Zilberg, S. The Nature of the S_1/S_0 Conical Intersection of Fulvene. *Chem. Phys.* **2006**, *325*, 251.

(39) Schlegel, H. B. Exploring Potential Energy Surfaces for Chemical Reactions: An Overview of Some Practical Methods. *J. Comput. Chem.* **2003**, *24*, 1514.

(40) Sicilia, F.; Bearpark, M. J.; Blancafort, L.; Robb, M. A. Quadratic Description of Conical Intersections: Characterization of Critical Points on the Extended Seam. *J. Phys. Chem. A* **2007**, *111*, 2182.

CT1000268